

Micrometer Positioning of a Trapped Ion in the Mode of an Integrated Optical Fiber

Tony Hyun Kim,^{1,*} Peter F. Herskind,¹ and Isaac L. Chuang¹

¹*Center for Ultracold Atoms, Department of Physics, Massachusetts Institute of Technology
77 Massachusetts Avenue, Cambridge, MA 02139*

(Dated: February 27, 2011)

We present a model as well as experimental results for a surface electrode radio-frequency Paul trap that has a circular electrode geometry well-suited for trapping of single ions and two-dimensional planar ion crystals. The trap design is compatible with microfabrication and offers a simple method by which the height of the trapped ions above the surface may be changed *in situ*. We demonstrate trapping of single $^{88}\text{Sr}^+$ ions over an ion height range of 200–1000 μm for several hours under Doppler laser cooling, and use these to characterize the trap, finding good agreement with our model.

PACS numbers: pacs

As quantum information processing (QIP) with trapped ions [1] evolves to include tens and hundreds of qubits, resources for trapping and qubit control are expected to impose significant overhead on the experimental infrastructure [2]. In this respect, the requirement of efficient light collection, laser cooling and qubit state manipulation of a large number of ions strongly motivates the integration of optics in ion traps [3, 4]. However, the potential benefits of integrated optics have long been overshadowed by the challenges of trapping ions in the proximity of dielectrics [5], as well as the difficulty of guaranteeing good spatial overlap of the trapped ion with the field mode of the integrated optical element.

In the past, there have been demonstrations of integration of bulk optics at ~ 10 mm distance [6–8] into traps that were of the linear four-rod Paul trap design. More recently, the integration of multi-mode optical fibers [9] and microscopic reflective optics [10] for the collection of ion fluorescence has been demonstrated in microfabricated surface-electrode designs. Complementing such work on light collection, the present Letter demonstrates light delivery in a surface-electrode point Paul trap through an integrated single-mode (SM) fiber for the 674 nm quadrupole transition of trapped $^{88}\text{Sr}^+$ ions. A key contrast between previous and current work is in the physical characteristics of the optical mode. Whereas light collection is achieved by the nearby placement of a high numerical aperture (NA) element in the vicinity of the ion's isotropic fluorescence, single-mode light delivery through an optical fiber involves a highly-directional Gaussian beam with mode diameters typically in the micron range. These dimensions place stringent demands on the relative alignment of the trapping fields and the integrated structure. Future developments in optics integration, such as the inclusion of lensed fibers for faster gate times and optical trapping of ions [11], or microcavities for ion-cavity quantum electrodynamics (cQED) experiments, will place even further demands on the precise construction of the ion-mode overlap. Building upon previous work in translation of a trapped ion using segmented rf electrodes [9, 12, 13], we demonstrate for the

first time micron-scale, micromotion-free positioning of the ion in the horizontal plane of a surface-electrode ion trap.

We approach the challenge of integrated light delivery by using the fiber itself as part of the trap structure. Figure 1(a) shows a schematic of the ion trap design, which is a modified version of the surface-electrode point Paul trap that was described recently [13]. The center, grounded electrode has a diameter of 1.0 mm. The elliptical rf pad has a major-axis diameter of 5.9

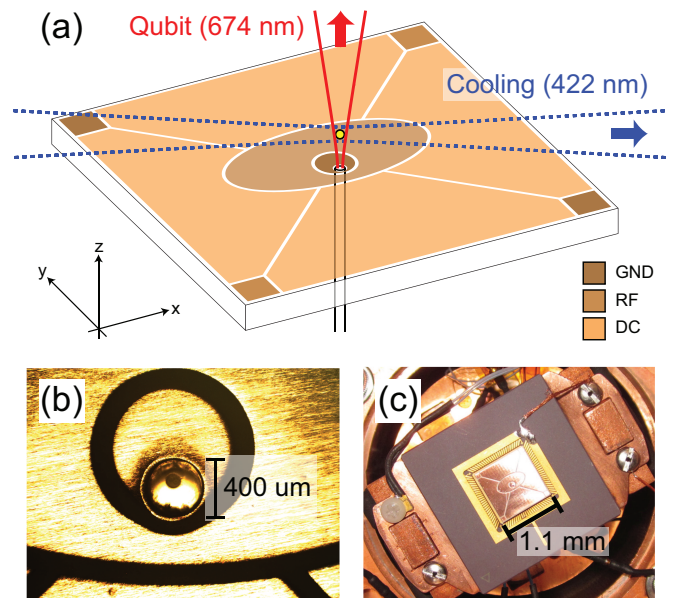


FIG. 1. (Color online) (a) A schematic of the surface-electrode ion trap with an integrated optical fiber for light delivery. The qubit laser is delivered axially (along \hat{z}) through the integrated fiber, while photoionization and Doppler cooling beams are brought radially (along $\hat{x} - \hat{y}$); (b) The alignment of the optical ferrule with respect to the trap electrodes. The ferrule is rotated until the fiber core is aligned with the minor axis of the trap; (c) Image of the fiber-integrated trap mounted on the CPGA and installed on the 8 K basplate of the closed-cycle cryostat.

mm and a minor-axis diameter of 2.8 mm, and is shifted with respect to the center of the ground electrode by $500\ \mu\text{m}$. These dimensions achieve an ion height of $670\ \mu\text{m}$. Asymmetries uniquely define the principal axes of the trap, which are tilted by 28° in the yz -plane for efficient cooling and micromotion compensation. The side electrodes are used for DC compensation of the ion, as well as radial translation of the rf node by use of additional rf voltages. Copper trap electrodes are defined on a printed circuit board (PCB) fabricated by Hughes Circuits on 0.8 mm-thick Rogers 4350, and also includes a $400\ \mu\text{m}$ -diameter plated via in the center electrode for the insertion of an optical ferrule. The $300\ \mu\text{m}$ offset of the ferrule via with respect to the ground electrode accounts for the displacement of the trapping point that accompanies the shift of the elliptical rf pad.

The optical fiber is SM for 674 nm (OZ Optics, PMJ-3A3A-633-4/125-3-10-1), and has a cladding diameter of $125\ \mu\text{m}$ and a core diameter of $3 \pm 0.5\ \mu\text{m}$. The fiber is conventionally prepared (i.e. cured in F112 fiber epoxy and polished) in a stainless steel SMA ferrule whose tip has been machined to the proper diameter for mating with the via of the PCB. The incorporation of the ferrule provides mechanical robustness for the subsequent assembly and install. The attachment of PCB and ferrule is performed under an optical microscope, as shown in Figure 1(b) where gross imprecision in the machining of the ferrule is evident in the form of $70\ \mu\text{m}$ nonconcentricity between the fiber and the ferrule. The ferrule is rotated with respect to the PCB in order to place the fiber core roughly along the minor axis of the trap, and was cured using cyanoacrylate adhesive. According to numerical simulation of the trap design, the final placement of the fiber core along deviates by about $50\ \mu\text{m}$ from the predicted trap location.

The fiber-integrated trap is installed on a ceramic pin grid array (CPGA) and mounted on the 8K baseplate of the closed-cycle cryostat [14] as shown in Figure 1(c). The fiber is routed through a hole in the CPGA and through a hole in a flange of the vacuum chamber, where it is sealed in place with TorrSeal UHV epoxy. (The epoxy is applied over the $900\ \mu\text{m}$ -diameter PVC jacket of the fiber.) The trap is operated at a typical rf frequency of $2\pi \cdot 6\ \text{MHz}$ and 250 Vpp amplitude, achieving secular frequencies of $\omega_{z'} = 2\pi \cdot 410\ \text{kHz}$, $\omega_x = 2\pi \cdot 240\ \text{kHz}$, $\omega_{y'} = 2\pi \cdot 170\ \text{kHz}$. We produce $^{88}\text{Sr}^+$ ions by resonant photoionization, which are then Doppler cooled on the $5S_{1/2} \leftrightarrow 5P_{1/2}$ transition at 422 nm, while simultaneously driving the $4D_{3/2} \leftrightarrow 5P_{1/2}$ transition at 1092 nm [see $^{88}\text{Sr}^+$ level diagram in Fig. 2(a)]. Ion fluorescence at 422 nm is collected by a 0.5 NA lens inside the chamber and imaged onto a CCD camera and a photomultiplier tube (PMT), both with individual ion resolution. We ensure that the ions are located at the nodal point of the rf field by minimizing the micromotion amplitude using the correlation measurement technique described in Ref.

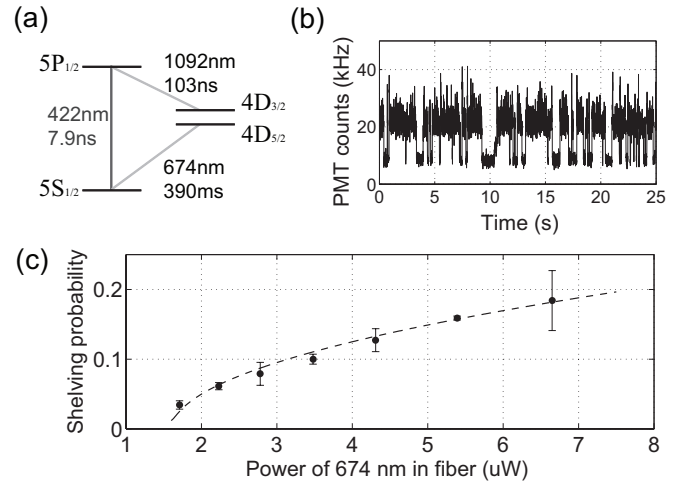


FIG. 2. (a) The level structure of $^{88}\text{Sr}^+$; (b) Telegraph log of a single trapped ion as it is shelved into the dark $4D_{5/2}$ state by the 674 nm fiber light; (c) Increase in the occupation of the dark state as a function of 674 nm power coupled to the trap fiber.

[15]. As the Doppler beam has nonzero projection along all three principal axes of the pseudopotential, the ion is positioned on the rf node exactly when the micromotion amplitude is eliminated.

The $5S_{1/2} \leftrightarrow 4D_{5/2}$ quadrupole transition is of particular interest for QIP with trapped ions as it forms the basis for the qubit in several implementations [1]. The ability to deterministically manipulate the ion on this transition using integrated light delivery is therefore of importance to large-scale QIP applications. As a simple demonstration of the interaction between the fiber mode and the ion, we send light at 674 nm through the fiber and observe the rate at which the ion is transferred to the metastable $4D_{5/2}$ state, while the ion is radially illuminated by the 422 nm and 1092 nm. Upon shelving the ion to the $4D_{5/2}$ state, no 422 nm photons are scattered, and the ion remains dark until it decays spontaneously back to the $5S_{1/2}$ state. Such telegraph scans of a single ion is shown in Fig. 2(b). The interaction strength on the $5S_{1/2} \leftrightarrow 4D_{5/2}$ transition can be quantified in terms of shelving probability, by computing the statistics of dark periods over a long (1 minute) measurement period. Fig. 2(c) shows the increase in shelving probability as a function of 674 nm power coupled to the trap fiber.

In the current instance of the fiber-integrated trap, the fiber mode size at the location of the ion is expected to be few tens of micrometers whereas the mechanical assembly of the ferrule and PCB resulted in an ion-fiber displacement of about $50\ \mu\text{m}$. Such offsets in the relative positioning of a trapped ion and an optical mode can dramatically diminish the interaction strength in cQED experiments. Previous work on this problem have often utilized a technically challenging setup in which the trap

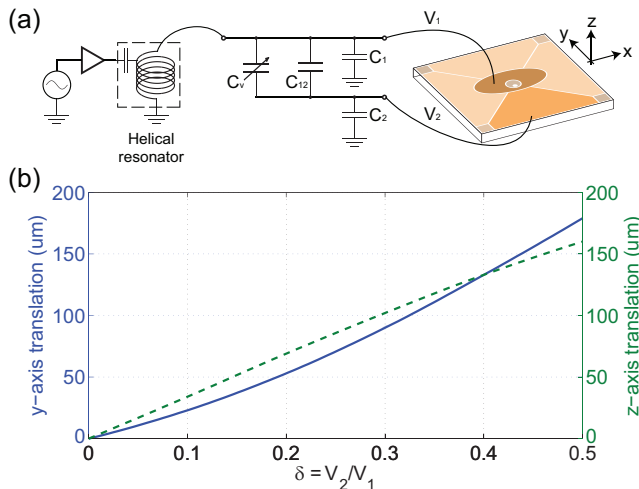


FIG. 3. (Color online) (a) A circuit model for implementing two in-phase rf drives through a capacitive network. Variable capacitor C_v is used to adjust the ratio of rf amplitudes $\delta = V_2/V_1$; (b) Numerically computed translation of the rf node from the single-rf trapping point as a function of δ . Solid blue curve shows radial (\hat{y}) displacement, while dashed green line shows axial (\hat{z}) displacement.

electrodes were adjusted mechanically [16], which is inapplicable when elements are integrated directly onto the trap structure. On the other hand, translation of the ion position by DC potentials suffers from increased micromotion as the ion is displaced from the node of the trapping rf field, which lead to broadening of the atomic transitions, thereby significantly limiting the usefulness of DC translation [15].

In contrast, the trapped ion can be translated by the use of segmented rf electrodes without incurring micromotion. For this scheme, it is important to maintain either perfect in-phase or out-of-phase drives for the multiple rf sources, as any other relative phase will result in excess micromotion. A simple way to achieve in-phase drive is to use a network of capacitors to couple a single rf source onto multiple electrodes, as shown in Figure 3(a). Capacitances C_1 and C_2 are intrinsic to the trap electrodes and chamber wiring, as is C_{12} , the intrinsic capacitive coupling between the two electrodes. We introduce a mechanically tunable capacitor $C_v = 0.5 - 30$ pF in order to adjust the coupling amplitude. Because the ion-fiber displacement lies predominantly along the minor axis of the trap, we have introduced the second rf on a side electrode on the minor axis. The extent of ion translation is parameterized by the ratio of rf amplitudes $\delta = V_2/V_1$, and the displacement of the rf node from the initial trapping point as a function of δ is shown in Fig. 3(b). Experimental verification of our numerical modeling was shown in previous work with the symmetric point Paul trap [13]. The rf amplitudes are monitored by a matched pair of capacitive dividers directly on V_1

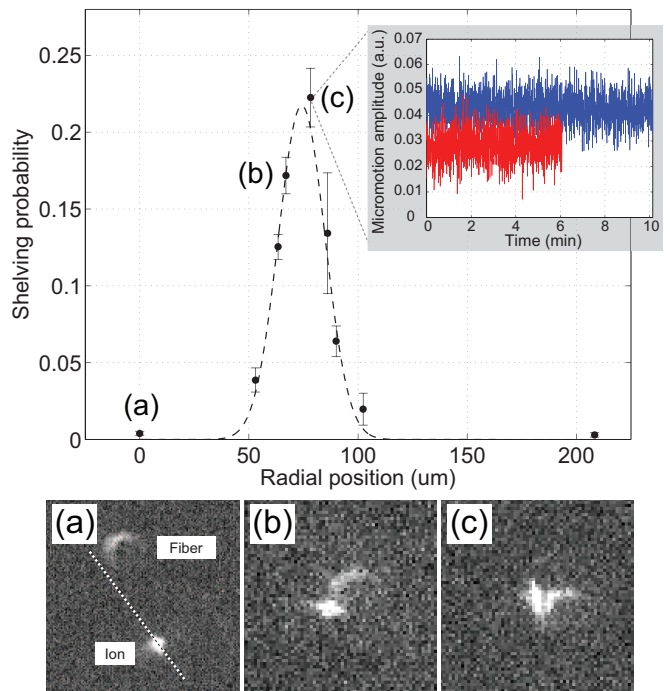


FIG. 4. (Color online) Measurement of the mode profile of the integrated fiber. The ion is translated using the technique of segmented rfs over the fiber mode along the minor axis of the trap. Dashed lines show a fit to a Gaussian profile, centered at $74.5 \pm 0.5 \mu\text{m}$. CCD image (a) shows the relative positioning of the ion and an unfocused image of the fiber facet under single-rf, where a dashed line indicates the minor axis of the trap. Images (b) and (c) show the relative positioning when the ion is brought closer to the maximum of the fiber mode. Inset shows a time log of the ion's micromotion amplitude with (red, short segment) and without (blue, long segment) $125 \mu\text{W}$ of fiber light when the ion is positioned at the peak of the fiber mode.

and V_2 , with overall detector quantization error of 2 Vpp.

Figure 4 shows the result of translating the ion across the mode of the integrated fiber using the rf method. The graph shows the shelving probability into the dark $4D_{5/2}$ state versus ion position as measured from the initial trapping point of single rf. The images (a), (b) and (c) show the ion displaced relative to the (unfocused) image of the fiber. Based on these measurements of the mode profile, we then find that the original trap location was offset from the mode by -74.5 ± 0.5 microns along the minor axis of the trap. Using an estimate of 2 V in rf voltage measurement error, we then find that points (a), (b) and (c) are offset $-74.5 \pm 1.6 \mu\text{m}$, $-7.5 \pm 3.0 \mu\text{m}$ and $3.8 \pm 3.2 \mu\text{m}$ from the fiber mode, respectively. Additionally, we have trapped and compensated ions as far as $500 \mu\text{m}$ away from the initial trapping point (by shorting V_1 and V_2), verifying the significant dynamic range of the rf translation technique. Given a particular application, sensitivity and dynamic range of the rf scheme, as

well as the precise trajectory, can be optimized through appropriate electrode design.

With the ion tuned over the fiber mode, we have looked for effects of dielectric charging by the 674 nm fiber light. The ion was illuminated by 125 μW of 674 nm trap light while being simultaneously repumped out of the dark $4^2D_{5/2}$ state on the 1033 nm $4D_{5/2} \leftrightarrow 5P_{3/2}$ transition. The amplitude of ion micromotion was recorded for several minutes under different conditions of fiber light. We find similar constancy of the micromotion amplitude, thereby implying no detectible charging of the dielectric due to activation of fiber light at 700–800 μm ion height.

In conclusion, we have developed and verified a process for the integration of an optical fiber with a surface-electrode ion trap that is technically simple and mechanically robust. While we have incorporated a single-mode, step-index fiber for the delivery of 674 nm for the $^{88}\text{Sr}^+$ ion, the assembly process is compatible with other fiber systems, such as lensed fibers that achieve very high intensities for faster gate times, endlessly single-mode photonic crystal fibers which can propagate all relevant trapping and manipulation lasers through a single integrated port, or hollow-core fibers that may permit the efficient coupling of ion systems to neutral atoms at opposite ends of the fiber [17].

The ease of trap assembly is achieved by the development of an independent technique for the *in situ* positioning of the trapped ion. We have demonstrated micrometer positioning of the ion along the horizontal plane of a surface-electrode ion trap, and have optimized the ion-fiber coupling despite an initial $74.5 \pm 0.5 \mu\text{m}$ mismatch due to the assembly of the trap. The positioning ability will be important in other types of integration, such as the coupling of a trapped ion to superconducting devices on the surface of a cryogenically operated trap [18]. Moreover, there is a clear analogy between the Gaussian mode of the integrated fiber with the optical mode of integrated microcavities for proposed cavity QED experiments [10], and the technique of segmented rfs could be crucial for attaining strong coupling between a single trapped ion and a cavity photon. An integrated trap that utilizes the fiber facet as one of the mirrors of an optical cavity could serve as a node in a distributed QIP architecture where the photon state can be extracted through the integrated fiber [19].

We expect the *in situ* control of the ion position to be a useful general technique for future experiments with surface-electrode ion traps. The ability to vary the ion height without incurring micromotion would be of tremendous value in the search for the origin of anomalous heating in ion traps [20, 21]. For this application, the integrated fiber permits study of the heating dynamics along the direction normal to the trap surface, in addition to the radial axis that is more commonly investigated. Furthermore, the ion may be placed over vari-

ous materials on the surface of a single trap, in order to study material dependences without introducing random errors associated with the fabrication of individual trap samples.

T.H.K. was supported by the Siebel Scholar Foundation and the Chorafas Foundation. P.F.H. is grateful for...

* kimt@mit.edu

- [1] R. Blatt and D. Wineland, *Nature*, **453**, 1008 (2008).
- [2] J. Kim, S. Pau, Z. Ma, H. R. McLellan, J. V. Gates, A. Kornblit, R. E. Slusher, R. M. Jopson, I. Kang, and M. Dinu, *Quantum Information & Computation*, **5**, 515 (2005).
- [3] J. Kim and C. Kim, *Quantum Information & Computation*, **9**, 0181 (2009).
- [4] E. W. Streed, B. Norton, J. Chapman, and D. Kielpinski, *Quantum Information & Computation*, **9**, 0203 (2009).
- [5] M. Harlander, M. Brownnutt, W. Hansel, and R. Blatt, *New Journal of Physics*, **12**, 093035 (2010).
- [6] M. Keller, B. Lange, K. Hayasaka, W. Lange, and H. Walther, *Nature*, **431**, 1075 (2004).
- [7] P. F. Herskind, A. Dantan, J. P. Marler, M. Albert, and M. Drewsen, *Nature Physics*, **5**, 494 (2009).
- [8] G. Shu, N. Kurz, M. Dietrich, and B. B. Blinov, *Phys. Rev. A*, **81**, 042321 (2010).
- [9] A. P. VanDevender, Y. Colombe, J. Amini, D. Leibfried, and D. J. Wineland, *Physical Review Letters*, **105**, 023001 (2010).
- [10] P. Herskind, S. X. Wang, M. Shi, Y. Ge, M. Cetina, and C. I. L., arXiv:1011.5259v1 (2010).
- [11] C. Schneider, M. Enderlein, T. Huber, and T. Schaetz, *Nature Photonics*, **4**, 772 (2010).
- [12] P. F. Herskind, A. Dantan, M. Albert, J. P. Marler, and M. Drewsen, *Journal Of Physics B-Atomic Molecular And Optical Physics*, **42**, 154008 (2009).
- [13] T. Kim, P. Herskind, T. Kim, J. Kim, and C. I. L., *Phys. Rev. A*, **82**, 043412 (2010).
- [14] P. B. Antohi, D. Schuster, G. M. Akselrod, J. Labaziewicz, Y. Ge, Z. Lin, W. S. Bakr, and I. L. Chuang, *Rev. Sci. Instrum.*, **80**, 013103 (2009).
- [15] D. J. Berkeland, J. D. Miller, J. C. Bergquist, W. M. Itano, and D. J. Wineland, *Journal Of Applied Physics*, **83**, 5025 (1998).
- [16] D. R. Leibbrandt, J. Labaziewicz, V. Vuletic, and I. L. Chuang, *Physical Review Letters*, **103**, 103001 (2009).
- [17] M. Bajcsy, S. Hofferberth, V. Balic, T. Peyronel, M. Hafezi, A. Zibrov, V. Vuletic, and M. D. Lukin, *Phys. Rev. Lett.*, **102**, 203902 (2009).
- [18] S. X. Wang, Y. Ge, J. Labaziewicz, E. Dauler, K. Berggren, and C. I. L., *Applied Physics Letters*, **97**, 244102 (2010).
- [19] J. I. Cirac, P. Zoller, H. J. Kimble, and H. Mabuchi, *Physical Review Letters*, **78**, 3221 (1997).
- [20] L. Deslauriers, S. Olmschenk, D. Stick, W. K. Hensinger, J. Sterk, and C. Monroe, *Physical Review Letters*, **97**, 103007 (2006).
- [21] J. Labaziewicz, Y. F. Ge, P. Antohi, D. Leibbrandt, K. R. Brown, and I. L. Chuang, *Physical Review Letters*, **100**, 013001 (2008).